

# Long Chain Polyamides: Influence of Methylene Sequence Length and External Forces on Structural Features

Rene Sattler, Varun Danke, and Mario Beiner\*

Crystallographic studies on a series of even–even polyamides PA10.*n* (12, 14, 16, and 18) with variable methylene sequence length ( $n - 2$ ) are performed. Temperature-dependent X-ray diffraction studies show that a triclinic  $\alpha$  phase is the preferred polymorph after slow cooling to room temperature like in many other even–even polyamides. For PA10.12 and PA10.14 the pseudo-hexagonal high temperature phase  $\gamma$  is observed between the Brill transition temperature  $T_B$  and melting point  $T_M$ . For both higher members a distinct Brill transition is absent below  $T_M$ . The influence of temperature on the packing state of the stems during cooling is discussed and compared to related polymers. An analysis of well oriented crystalline states in annealed fibers reveals that the crystalline state achieved under ambient conditions is influenced by external forces due to small energetic differences between different  $\alpha$  and  $\beta$  polymorphs. All PA10.*n* samples show in the fiber-oriented state a prominent  $\beta$  polymorph which is dominant in PA10.12 and PA10.14 but superimposed with a significant  $\alpha$  fraction in both higher members. The consequences of changes in the polymorphic state under the influence of external forces for crystalline states achieved under application relevant processing conditions are considered.

1930s, they have found numerous applications in a variety of markets ranging from automotive to consumer goods. Despite being well established materials of choice for a variety of applications, and a focus of numerous pioneering works since the 1940s,<sup>[1,2]</sup> the structural features of polyamides are extremely complex and in part not entirely understood. The presence of numerous polymorphic states, temperature dependent solid–solid phase transitions and their sensitive dependence on methylene sequence lengths as well as molecular architecture are some of the facets which make structural evaluation difficult.<sup>[3,4]</sup> Crystallization control on the other hand, offers an attractive possibility to tune the material properties. A common feature of all polyamides is the existence of hydrogen bonds between two neighboring amide groups resulting in a regular spatial arrangement of the chains. The amide group density governs all features including moisture absorption, crystallinity, melting points as well as all

## 1. Introduction

Linear aliphatic polyamides are an important class of semi-crystalline polyamides and since their discovery in the early


significant application relevant mechanical properties such as modulus, impact strength, etc.<sup>[5,6]</sup> The arrangement of amide groups next to each other supported by hydrogen bonding between neighboring chains leads to layered structures in the crystalline state formed by an alternating arrangement of methylene sequences and amide groups. The packing arrangement within the crystal is found to depend on several factors such as I) the chemical nature—AABB (formed by polycondensation of a diamine with a diacid) versus AB (formed by ring opening polymerization of a lactam or a  $\omega$ -amino acid). II) Architecture of the chain—odd even effects based on the number of methylene units in the diamine, diacid and the lactam.<sup>[7]</sup> III) Kinetic factors such as cooling rates and crystallization temperature, temperature induced crystalline phase transitions, the most common being the Brill transition.<sup>[8–11]</sup> IV) Effect of external shear forces and orientation.<sup>[12–15]</sup>

Although there are ongoing debates about the exact nature of crystalline packing with respect to the chain configurations, unit cells and angles, the occurrence of layered structures either in the form of sheets ( $\alpha$  and  $\beta$  phases) or mesophase (pseudo-hexagonal phase  $\gamma$ ) are widely accepted models.<sup>[16]</sup> In early crystallographic studies the room temperature polymorphs of PA 6.6 and PA 6.10 were studied based on drawn fibers and double-oriented strips by Bunn and Garner.<sup>[1]</sup> Two polymorphs are reported in this pioneering paper being the dominating triclinic

R. Sattler, M. Beiner  
 Fraunhofer Institute for Microstructure of Materials and Systems IMWS  
 Walter Hülse Str. 1, D-06120 Halle (Saale), Germany  
 E-mail: mario.beiner@imws.fraunhofer.de

R. Sattler, M. Beiner  
 Faculty of Natural Sciences II  
 Martin Luther University of Halle-Wittenberg, D-06099 Halle (Saale),  
 Germany

V. Danke  
 Evonik Operations GmbH  
 Research, Development & Innovation  
 Paul-Baumann-Str. 1, D-45722 Marl, Germany

 The ORCID identification number(s) for the author(s) of this article can be found under <https://doi.org/10.1002/macp.202200433>

© 2023 The Authors. Macromolecular Chemistry and Physics published by Wiley-VCH GmbH. This is an open access article under the terms of the Creative Commons Attribution-NonCommercial-NoDerivs License, which permits use and distribution in any medium, provided the original work is properly cited, the use is non-commercial and no modifications or adaptations are made.

DOI: 10.1002/macp.202200433

$\alpha$  phase and the triclinic  $\beta$  phase (space group  $P\bar{1}$ ). The amide groups placed regularly along the backbone are reported to form hydrogen bonded sheets along the *ac*-plane in both polymorphic states. Both polymorphs are characterized by prominent (100) and (010) reflections (the later superimposed with the (110) reflection) in the WAXS region corresponding to spacings of  $d_{100} = 0.44$  nm and  $d_{010} = 0.37$  nm. This indicates that the stem-to-stem distances in  $\alpha$  and  $\beta$  polymorphs are quite similar. The (100) spacing corresponds to the distance between lattice planes in the hydrogen bonded direction while the (010) spacing is the distance between lattice planes in the non-hydrogen bonded direction. The angle  $\beta$  between the *a* and *c* axes is commonly found to be about  $77^\circ$  related to a continuous shift between neighbored stems in such a way that the oxygen atom of one stem is near the NH group of the next enabling a hydrogen bond to be formed. Additional (00*l*) spacings in the intermediate angle region (MAXS) indicate the existence of layered structures with alternating methylene and thin amide layers. Main difference between  $\alpha$  and  $\beta$  phases is the relative shift between the non-hydrogen-bonded stems. In the  $\alpha$  phase the amide groups are displaced progressively by 0.355 nm resulting in an angle of about  $\alpha = 49^\circ$  between *b* and *c* axes of the unit cell. In the  $\beta$  phase the non-hydrogen-bonded stems are displaced in an alternating up and down arrangement along the *bc*-plane resulting in  $\alpha = 90^\circ$ . The resulting unit cell of the  $\alpha$  phase is found to be triclinic with  $a = 0.49$  nm,  $b = 0.54$  nm,  $\alpha = 49^\circ$ ,  $\beta = 77^\circ$ , and  $\gamma = 64^\circ$  and contains a single monomer. The unit cell of the  $\beta$  phase has dimensions of  $a = 0.49$  nm,  $b = 0.80$  nm,  $\alpha = 90^\circ$ ,  $\beta = 77^\circ$ , and  $\gamma = 67^\circ$  but contains two monomers.<sup>[1]</sup> These values remain constant in both polymorphs irrespective of the length of the methylene sequence.<sup>[16]</sup> Only the *c* value parallel to the chains (stems) is dependent on the length of the methylene sequences commonly assumed to be in the all-trans state.<sup>[1]</sup>

Atkins et al. have investigated various even–even polyamides *m.n* (with  $m = 2$ –12 and  $n = 4$ –12) in detail and refined the structures proposed by Bunn and Garner for these polymers.<sup>[7]</sup> It is shown that the members of the series with  $m > 2$  can form also two different hydrogen bonded sheet arrangements. That is, a progressive shift of the units forming hydrogen bonds (*p*-sheets,  $\beta = 77^\circ$ ) as proposed by Bunn and Garner<sup>[1]</sup> or alternating (up-and-down) shift of units forming hydrogen bonds (*a*-sheets,  $\beta = 90^\circ$ ) along the *ac*-plane, resulting in four different possible phases  $\alpha_p$ ,  $\alpha_a$ ,  $\beta_p$  and  $\beta_a$ . In the  $\alpha_p$  phase a “fully saturated hydrogen-bonded sheet arrangement” is achieved and therefore the  $\alpha_p$  phase is most likely to be formed. However, a mixed crystalline state containing  $\alpha_p$  phase with a certain fraction of  $\beta_p$  is also often observed.<sup>[7]</sup> The  $\alpha_a$  and  $\beta_a$  phase has been preferentially found in symmetric polyamides like PA 8.10 or PA10.12 probably due to the symmetrical architecture of the monomeric units.<sup>[7]</sup>

Besides the two room temperature phases  $\alpha$  and  $\beta$ , a high temperature phase  $\gamma$  occurs in several even–even polyamides above the so called Brill transition temperature  $T_B$ . The polymorph  $\gamma$  has a (pseudo)hexagonal structure indicated by a single WAXS reflection corresponding to a spacing of 0.42 nm.<sup>[8–11]</sup> This is a special version of the situation observed for  $\alpha$  and  $\beta$  phases with identical spacings in (100) and (010) direction including an angle of  $60^\circ$ . It is discussed that 2D hydrogen bonded sheets transform

to a 3D hydrogen bonded arrangement if the  $\gamma$  phase is formed at  $T_B$ .<sup>[7,9]</sup>

In a recent paper by Lotz, further structures of even–even polyamides were proposed and already known structures were validated via molecular modeling and simulations.<sup>[16]</sup> Additional structures introduced are pleated and rippled sheets featuring twisted torsion angles at the amide CO-NH bonds resulting in slightly deviating spacings in the WAXS range.<sup>[16]</sup>

Interestingly, layer-like packing has also been observed in a relatively new class of polymers referred to as precision polyethylenes. These polymers contain regularly placed functional groups such as alkyl branches,<sup>[17]</sup> sulphones,<sup>[18]</sup> halogens,<sup>[19]</sup> and so on, along a linear polyethylene chain. The functional groups or “defects” as called in some studies may in addition promote supramolecular interactions such or  $\pi$ – $\pi$ -stacking or hydrogen bonding similar to polyamides, often leading to the formation of layered structures where methylene layers and layers containing “defects” alternate. Polymorphism is commonly observed in such systems with the methylene sequence lengths playing a major role in defining the molecular order within the crystalline phase.<sup>[20]</sup> This behavior can be understood as a result of interplay between the van der Waals interaction between methylene sequences and the supramolecular interactions, creating some sort of a competing effect, as the native packing states of  $\text{CH}_2$  units and the interacting functional groups may not be similar. One can understand this as an energetic compromise leading to metastable states which strongly depend on crystallization conditions. A general classification scheme was proposed wherein the individual sub-units methylene sequences and functional groups tend to pack independently resulting in different polymorphic states.<sup>[21]</sup> For example, the methylene sequences can be either be disordered, or can exhibit a native PE-like packing. On the other hand, the functional groups can show a preferred ordering, but prohibit the packing of methylene sequences on a PE-like lattice. The presence of the resulting highly ordered structures was shown in a recent publication.<sup>[22]</sup> Such independent packing tendencies are also observed in comb-like polymers with long alkyl side chains.<sup>[23–25]</sup> In these systems, the long-range ordered layered morphologies are commonly observed as long as one of the sub-units (that form the backbone or the side chain) is able to undergo crystallization. Hence, well defined layered structures have been also observed in case of completely amorphous backbones, for example, in atactic polymethacrylates<sup>[26]</sup> and regio-random polythiophenes.<sup>[27]</sup> If such structures melt, a demixing of the sub-units on the nanoscale, referred as nanophase separation, is often preserved even in the fully amorphous state due to specific intermolecular interactions between the sub-units.<sup>[28,29]</sup>

The focus of the work presented here is the influence of the methylene sequence lengths on the crystalline packing state in a series of even–even polyamides PA10.*n*, where *n* is either 12, 14, 16, or 18 and denotes the number of carbon atoms in the diacid used during the polycondensation. Such long chain polyamides (LCPAs) are considered as high-performance polymers and are a separate class of semi-crystalline aliphatic polyamide typically containing >10 methylene units per amide group. From the application perspective, they have significant advantages over conventional polyamides such as PA4.6, PA6, and PA6.6 such as enhanced low temperature toughness, chemical resistance, and low

**Table 1.** Monomers and thermal properties of PA10.*n*.

AABB polyamide	Diamine	Diacid	$T_g/^\circ\text{C}^a)$	$T_C/^\circ\text{C}$	$T_{m2}/^\circ\text{C}$
PA10.12	Decamethylene diamine	Dodecanedioic acid	47	162	192
PA10.14	Decamethylene diamine	Tetradecanedioic acid	37	144	185
PA10.16	Decamethylene diamine	Hexadecanedioic acid	36	145	180
PA10.18	Decamethylene diamine	Octadecanedioic acid	35	149	178

<sup>a)</sup> Taken from dynamic-mechanical measurements as shown in Figure S1, Supporting Information.

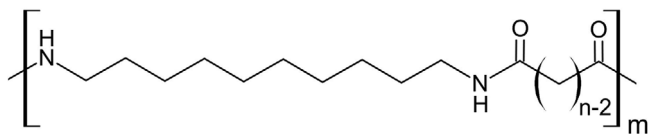


**Figure 1.** Chemical structure of polyamide 10.*n*.

moisture absorption due to lower amide group density. Of special interest are different crystalline polymorphs, the packing of the individual stems and sub-units within these polymorphs and the influence of external forces on the polymorphic state of these LCPAs. This is a crucial first step to enable efficient crystallization control during different processing conditions such as extrusion, injection molding, etc.

## 2. Experimental Section

### 2.1. Materials

A series of non-commercial even–even polyamides 10.*n* (with  $n = 12, 14, 16$  and  $18$ ) is investigated. The Polyamides 10.*n* were synthesized on a pilot scale reactor using a standard polycondensation reaction of decamethylene diamine with the respective dicarboxylic acid as shown in Table 1. Polycondensation of a diacid and diamine to yield so called AABB polyamides is a well-known and established state of the art.<sup>[6,30,31]</sup> The chemical structure of polyamide 10.*n* is shown in Figure 1.

Crystallization and melting temperatures,  $T_C$  and  $T_m$  respectively, were determined based on DSC measurements using a PerkinElmer DSC7 in a temperature range between  $-20$  to  $220$  °C. The specific heat capacity  $C_p$  is obtained from first cooling and second heating runs with rates of  $\pm 20$  K  $\text{min}^{-1}$ . Figure 2 shows the specific heat capacity  $C_p$  data for the investigated PA10.*n* series during the second heating run. Between 25 and 50 °C a step like feature was observed, which corresponded to a glass transition related to the amorphous polymer fraction. A well pronounced melting peak was observed between 175 and 200 °C in Figure 2 for all investigated PA10.*n* samples. This melting peak, labeled as  $T_{m2}$  here, was shifting as expected systematically to lower temperatures with increasing  $n$ . An additional melting peak like feature, labeled as  $T_{m1}$  here, was seen in particular in DSC heating scans for PA10.16 and PA10.18 above 125 °C. This feature indicates melting of a certain crystalline fraction

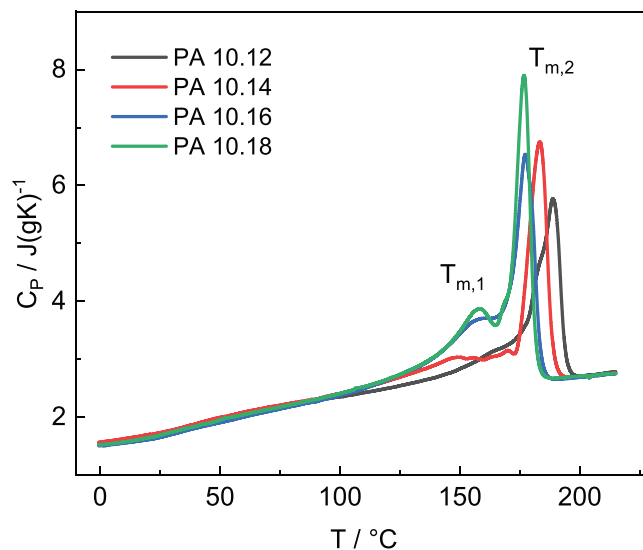


**Figure 2.** Specific heat capacity  $C_p$  of PA10.*n* obtained during heating between 0 and 220 °C. The heating rate is 20 K  $\text{min}^{-1}$ .

in this temperature range. The intensity of this peak at  $T_{m1}$  increases clearly with increasing  $n$ . The formation of two melting peaks in DSC measurements was in accordance with results reported in the literature and could be related to melting of crystals formed during cooling at ( $T_{m1}$ ) accompanied by re-crystallization or melting of the more perfect crystals at ( $T_{m2}$ ). The characteristic parameters obtained from DSC and additional dynamic-mechanical measurements are summarized in Table 1. Melting  $T_m$  as well as crystallization temperature  $T_C$  were determined as peak value in the second heating and first cooling run, respectively.

### 2.2. Preparation of Oriented Samples

Detailed investigations of the crystalline structure by X-ray diffraction required oriented samples. For that purpose shear oriented fibers were prepared by ram extrusion and subsequent cold drawing. Before ram extrusion the samples were dried in a vacuum oven under ambient pressure at 85 °C for 5 h. Afterward the fibers were extruded on a home-built setup for ram extrusion (for details see ref. [32]) at 190 °C with a shear rate  $\dot{\gamma}$  of 5  $\text{s}^{-1}$ . The fibers were subsequently further oriented 3 $\times$  drawing with a draw ratio of 3.75  $\text{min}^{-1}$  in the temperature chamber of a universal testing machine Zwick Z050 at 100 °C following a procedure proposed by Arimoto and co-workers in ref. [33]. After orientation, the fibers were annealed in a vacuum oven under ambient pressure at 130 °C for 10 h.

### 2.3. Structure Characterization Methods

#### 2.3.1. X-Ray Diffraction Measurements

The X-ray diffraction (XRD) experiments were performed in transmission mode using a SAXSLAB laboratory setup (Retros) equipped with an AXO microfocus X-ray source and an AXO

multilayer X-ray optic (ASTIX) as monochromator for Cu  $K_{\alpha}$  radiation ( $\lambda = 1.54 \text{ \AA}$ ). A DECTRIS PILATUS3 R 300K detector was used to record the 2D scattering patterns. The 2D XRD pattern were then integrated via SAXSGUI in order to get the 1D XRD pattern. The sample to detector distance was  $\approx 10 \text{ cm}$ . A twin pin-hole system was used for the measurements with an aperture size of  $\approx 0.9 \text{ mm}$  and  $\approx 0.4 \text{ mm}$ . Temperature-dependent scattering measurements on the as received samples were performed using a Linkam hot stage. The filaments were placed in a small hole in an aluminum disc having a diameter of 2 mm and a thickness of 4 mm. The used temperature range was  $T = 30 \text{ }^{\circ}\text{C}$  to  $T = 220 \text{ }^{\circ}\text{C}$  covered in steps of 10 K. The heating and cooling rate for ramping between isothermal measurements was  $10 \text{ K min}^{-1}$ , isothermal measurement time was 5 min. A first heating run (not shown) was performed to erase the thermal history of the materials. For a detailed analysis of the X-ray diffraction data, a peak deconvolution was applied by fitting the Bragg reflections as well as the amorphous halo with various Lorentzian functions as shown in Figure 3.

The degree of crystallinity  $\chi_c$  was estimated based on the ratio of the area of all Bragg reflections ( $\Sigma A_{hkl}$ ) to the total area of the XRD pattern ( $\Sigma A_{hkl} + A_{amo}$ ) in the WAXS region ( $7.5 \text{ nm}^{-1} < q < 20 \text{ nm}^{-1}$ ) according to

$$\chi_c = \frac{\Sigma A_{hkl}}{\Sigma A_{hkl} + A_{amo}} \quad (1)$$

The coherence length  $L$  was determined according to Scherrer's equation

$$L = \frac{K\lambda}{w_{hkl} \cos \theta_{hkl}} \quad (2)$$

with  $K = 0.9$  being the Scherrer constant,  $w_{hkl}$  being the full width at half maximum height in radiant and  $\theta_{hkl}$  the relevant Bragg angle.

## 3. Results

### 3.1. Ambient Temperature X-Ray Diffraction Data for Bulk Samples

Figure 4 shows X-ray diffraction pattern obtained by azimuthal integration of 2D scattering data for PA10. $n$  in the intermediate (MAXS) and wide angle (WAXS) region obtained at  $30 \text{ }^{\circ}\text{C}$  after slow cooling from melt.

In the MAXS region one can observe a reflection at  $\approx 3.7 \text{ nm}^{-1}$ , labeled as  $q_{002}$ , corresponding to layered superstructure which is commonly observed in polyamides. With increasing  $n$ ,  $q_{002}$  is shifting to lower values due to a longer  $\text{CH}_2$  sequence length. The corresponding spacing  $d_{002} = 2\pi/q_{002}$  is increasing from 1.2 nm for PA10.12 to 1.42 nm for PA10.18. Interestingly, lower and higher order reflections, labeled as  $q_{001}$  and  $q_{003}$ , appear and become prominent with increasing methylene sequence length. This can be explained by a transition from sheet symmetry in case of PA10.12 to more asymmetric layer dimensions within the unit cell for larger  $n$  values. It is argued that in case of PA10.12 the monomers and the unit cells are split exactly in the middle

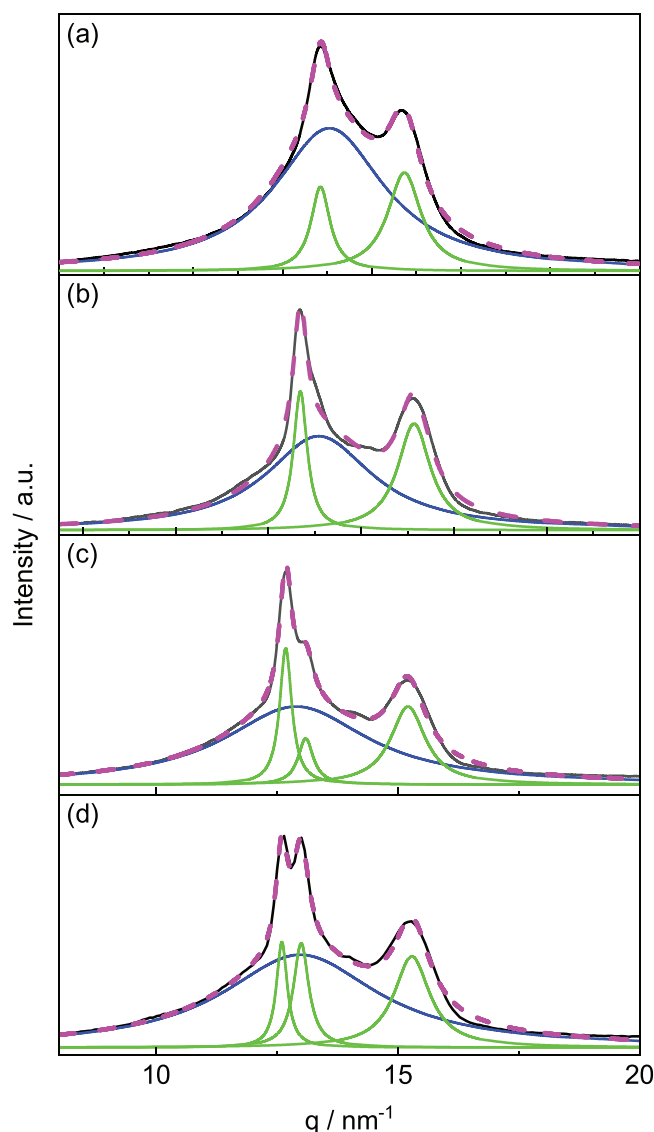


Figure 3. Peak deconvolution of data for a) PA10.12, b) PA10.14, c) PA10.16, and d) PA10.18 at  $30 \text{ }^{\circ}\text{C}$  taken after slow cooling from the molten state. The baseline corrected data is shown in black, amorphous halo in blue, Bragg reflections in green, and cumulative fit in pink dashed.

by planes containing amide groups with significantly higher electron density compared to that of the methylene sequences.<sup>[3,7]</sup> For slightly different  $n$  values the intensity of the  $q_{001}$  signal should be still weaker compared to the  $q_{002}$  intensity. However, this effect should diminish with increasing asymmetry. This can explain the increase of the  $q_{001}$  intensity with increasing  $n$  obviously quite well.

Two prominent reflections labeled as  $q_{100}$  and  $q_{010}$  occur in the WAXS region at  $\approx 14.3 \text{ nm}^{-1}$  and  $\approx 16.9 \text{ nm}^{-1}$ , respectively. The corresponding spacings are  $d_{100} = 0.44 \text{ nm}$  and  $d_{010} = 0.37 \text{ nm}$  as typically reported for the triclinic  $\alpha_p$  and  $\beta_p$  phase for even-even polyamides.<sup>[1,3,7,16,34–37]</sup> These reflections correspond basically to the distances between neighbored polyamide chains and are prominent indicators for crystalline packing. However, clear differences between  $\alpha$  and  $\beta$  phases are not reported in this

**Table 2.** Bragg spacings  $d_{hkl}$ , coherence length  $L_{100}$  and degree of crystallinity  $\chi_c$  of different PA10. $n$  at 30 °C after slow cooling from the melt.

	$d_{001}$ / nm	$d_{002}$ / nm	$d_{003}$ / nm	$d_{100}$ / nm	$d_{100\alpha}$ / nm	$d_{010}$ / nm	$L_{100}$ / nm	$\chi_c$ / %
PA10.12	–	1.20	–	0.44	–	0.38	11.11	24
PA10.14	–	1.26	–	0.44	–	0.37	19.77	30
PA10.16	2.66	1.32	0.89	0.44	0.43	0.37	18.80	30
PA10.18	2.85	1.42	0.94	0.44	0.43	0.37	22.64	39

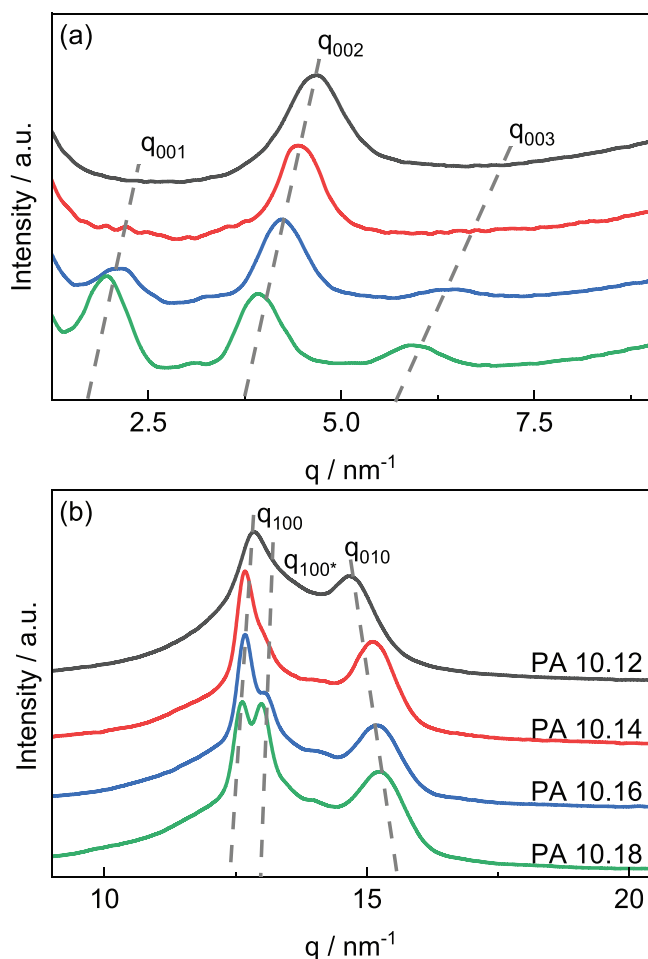


**Figure 4.** Integrated X-ray diffraction pattern of PA10. $n$  as function of the scattering vector  $q$  in the a) MAXS and b) WAXS region after slow cooling to 30 °C from the molten state. The patterns are shifted vertically for the sake of clarity.

regard.<sup>[1,16]</sup> The (100) reflection is commonly associated with the direction where H bonds between neighbored amide groups occur while the (010) reflection corresponds to the non-hydrogen bonded direction. Interestingly, a peak splitting of the  $q_{100}$  reflection arises and becomes more pronounced with increasing  $n$ , along with the appearance of  $q_{001}$  and higher order  $q_{003}$  in the MAXS range. The new second reflection is occurring at  $\approx 14.6$  nm<sup>-1</sup> which is labeled here by  $q_{100^*}$  assuming that it indicates the existence of another  $\alpha$  or  $\beta$  polymorph with slightly different unit cell dimensions. The occurrence of another strong reflec-

tion close to  $q_{100}$  related to another set of lattice planes seems to be more unlikely based on detailed considerations presented in ref. [1].

In order to determine the degree of crystallinity  $\chi_c$  and the coherence length  $L$ , a peak deconvolution analysis is performed for the X-ray diffraction data in the WAXS region. The Bragg spacings determined by this data evaluation method are given in **Table 2**. The degree of crystallinity  $\chi_c$  obtained from WAXS data is in the range 24% to 39% and comparable with values reported in literature.<sup>[9]</sup> It is noteworthy that both, degree of crystallinity  $\chi_c$  as well as coherence length  $L_{100}$  do increase systematically with increasing methylene sequence length. This indicates that the lateral size of crystalline regions increases with  $n$ .

### 3.2. Temperature-Dependent X-Ray Diffraction Pattern for Bulk Samples

The X-ray diffraction pattern for the investigated PA10. $n$  series measured during step-wise cooling are shown in **Figure 5**. At 220 °C all PA10. $n$  samples are in the molten state indicated by an amorphous halo centered at about  $\approx 12$  nm<sup>-1</sup>. A second broad peak occurs at  $\approx 5$  nm<sup>-1</sup>. This feature is observed close to the (002) reflection at lower temperature and is reminiscent of pre-peaks which are often observed in the amorphous state of nanophase-separated systems like comb-like polymers or precision polymers interpreted as an indication for nanophase separation, that is, demixing of incompatible sub-units in molten state.<sup>[21,28,29]</sup>

Crystallization of PA 10.12 starts during cooling at 180 °C indicated by the appearance of a Bragg reflection labeled as  $q_{ht}$  at 13.22 nm<sup>-1</sup> corresponding to the high temperature ( $\gamma$ ) phase discussed to have a (pseudo)hexagonal structure in other polyamides (Figure 5a). Along with the peak at  $q_{ht}$  a  $q_{002}$  reflection arises at 4.63 nm<sup>-1</sup> in the MAXS region. The corresponding Bragg spacings are  $d_{002} = 1.36$  nm and  $d_{ht} = 0.42$  nm. The reflection at  $q_{ht}$  is splitting upon further cooling into two reflections,  $q_{100}$  and  $q_{010}$ , below the Brill transition temperature  $T_B$  at about 90 °C. These reflections are commonly found for  $\alpha$  and  $\beta$  phases of polyamides.<sup>[7,16,34–38]</sup> The Brill transition can be clearly identified in **Figure 6a** showing the temperature-dependent evolution of all spacings related to the WAXS region for PA 10.12 from cooling and subsequent heating run. The spacing  $d_{100}$  is seemingly less dependent on temperature as compared to  $d_{010}$ . The differences between heating and cooling run in the Brill transition region are weak. It is important to note here that there is neither a significant change in the  $d_{002}$  spacing at the Brill transition temperature (cf. Figure S2, Supporting Information) nor a significant peak in DSC scans in the temperature range near  $T_B$ .

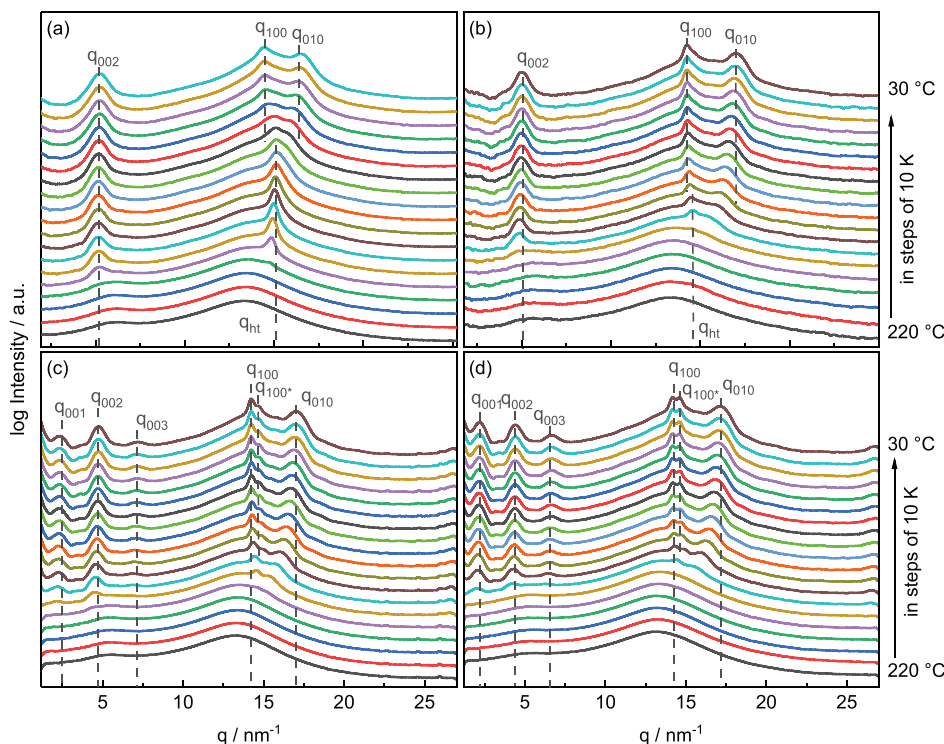


**Figure 5.** Integrated X-ray diffraction pattern of a) PA10.12, b) PA10.14, c) PA10.16, and d) PA10.18 determined during step-wise cooling from 220 to 30 °C. The corresponding reflections are labeled. The dashed lines indicate the peak positions at 30 °C.

The lack of a significant peak in the DSC scans indicates an extremely small transition enthalpy being often seen for solid-solid phase transitions.

Related data from temperature-dependent WAXS measurements on PA10.14 in Figures 5b and 6b show quite similar features and trends but also specific differences. First difference compared to PA10.12 is that crystallization during cooling and melting during heating occurs at lower temperatures in accordance with lower  $T_C$  and  $T_m$  values from DSC. Second difference is that the Brill transition is obviously shifted to a much higher temperature  $T_B$ . The merging of (100) and (010) reflections in case of PA10.14 appears near 150 °C, which is very close to the crystallization temperature  $T_C$ . This is indicated in the WAXS pattern close to  $T_C$  (Figure 5b) but more clearly seen in the temperature-dependence of  $d_{100}$  and  $d_{010}$  (Figure 6b).

The scattering pattern for PA10.16 and PA10.18 show clear differences compared to those for PA10.12 and PA10.14. In particular there are additional (001) and (003) reflections in the MAXS region as well as a splitting of the (100) reflection in the WAXS region (Figure 5c,d) as already mentioned above. In addition, there is no Brill transition below  $T_M$  for PA10.16 and PA10.18 although a certain tendency toward merging of (100) and (010) reflections with increasing temperature is still observed above 100 °C (Figure 6c,d). In the temperature range between 100 °C and  $T_M$  the spacings  $d_{100}$  and  $d_{010}$  differ significantly from their room temperature values being about 0.44 nm and 0.37 nm, respectively. This can be interpreted as indication for a shift of the Brill transition to temperatures above  $T$  for  $n > 14$  in the investigated PA10. $n$  series.

### 3.3. Diffraction Data for Fiber-Oriented Samples

In order to get additional insights toward understanding the crystalline structure of our PA10. $n$  samples, ram-extruded and subsequently drawn fibers have been investigated. The obtained 2D diffraction pattern for PA10.12 and PA10.18 measured at room temperature are presented in Figure 7. The dependence of the scattering intensity on the azimuthal angle  $\phi$  is given for the major reflections in Figure 8. Clear evidences for a high degree of orientation are observed. The scattering intensity of the (100) and (010) reflections is concentrated in horizontal direction, that is, highly intense arcs occur perpendicular to the fiber axis at  $\phi = 0$  and 180 °. The spacings ( $d_{100} \approx 0.44$  nm and  $d_{010} \approx 0.38$  nm) are quite similar to those for non-oriented samples in case of PA10.16 and PA10.18 while those for oriented PA10.12 and PA10.14 fibers ( $d_{100} \approx 0.43$  nm and  $d_{010} \approx 0.395$  nm) are slightly different from values for non-oriented samples. A detailed comparison of the scattering pattern of extruded and further cold drawn PA10.18 fibers with the corresponding bulk sample (Figure 9) shows clearly that significant changes regarding the (001) reflections occur during cold-drawing while the splitting of the (100) reflection is lost already in the extruded fibers.

Interestingly, the scattering intensity of the (002) reflection is located at the meridional position in the 2D pattern for PA10.12 and PA10.14 fibers (Figures 7 and 8). In case of PA10.16 and PA10.18 the azimuthal intensity distribution of the (002) reflection is indicating the coexistence of two phases. One can still see an intensity maximum at the meridional position but also two additional peaks which are tilted relative to the vertical direction in the 2D pattern. A peak analysis reveals a tilt of about

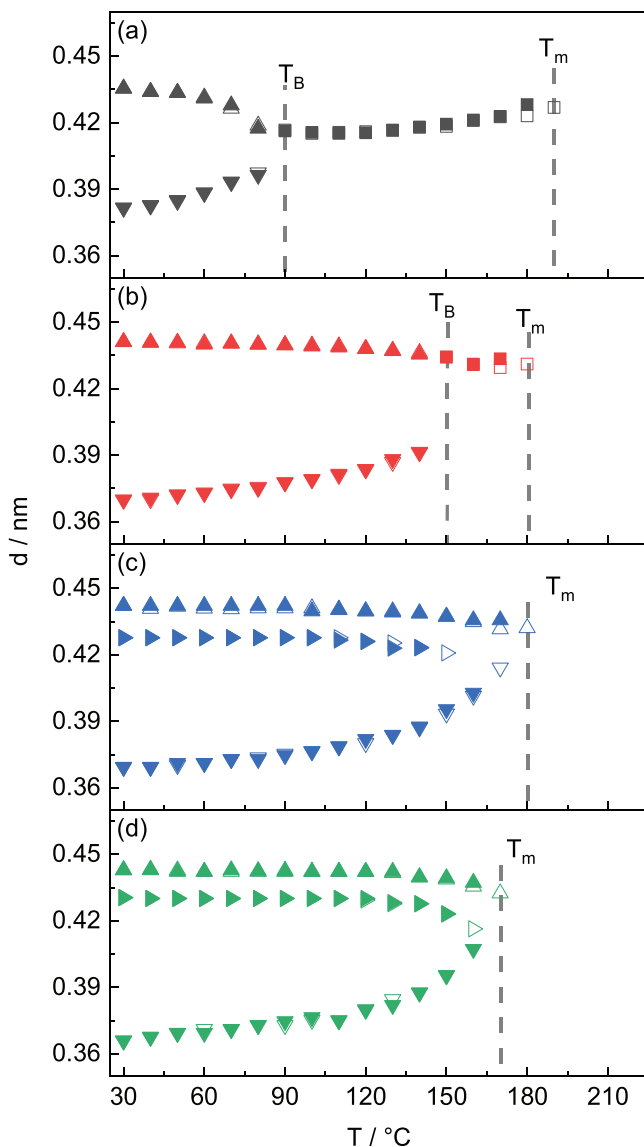


**Figure 6.** Evolution of  $d_{100}$  ( $\blacktriangle$ ),  $d_{010}$  ( $\blacktriangledown$ ),  $d_{100^*}$  ( $\blacksquare$ ) and  $d_{100^*}$  ( $\blacktriangleright$ ) in the WAXS region of a) PA10.12, b) PA10.14, c) PA10.16, and d) PA10.18 during cooling (full symbols) and second heating run (open symbols). Brill transition  $T_B$  and melting temperature  $T_m$  are indicated by vertical dashed lines.

$30^\circ$  relative the vertical direction. The  $q_{00l,v}$  values obtained for the reflections in vertical direction are smaller than those for the peaks related to tilted planes  $q_{00l,t}$  (Figure 10). This is quite clearly seen for the (002) and (003) reflections. The spacings  $2 \times d_{002,v}$  are for all PA10. $n$  samples larger than the  $2 \times d_{002}$  values for non-oriented samples grown in the absence of shear forces in temperature-dependent measurements and approach the fully stretched all-trans length of the main chains (Figure 11). The  $2 \times q_{002,t}$  values are very close to the  $2 \times d_{002}$  values from measurements made during step-wise cooling of bulk samples. Hence, the pattern with tilted (00l) reflections should indicate a more equilibrated structure, that is, the triclinic  $\alpha$  phase which are commonly reported for even-even polyamides at low temperatures.<sup>[7,16]</sup>

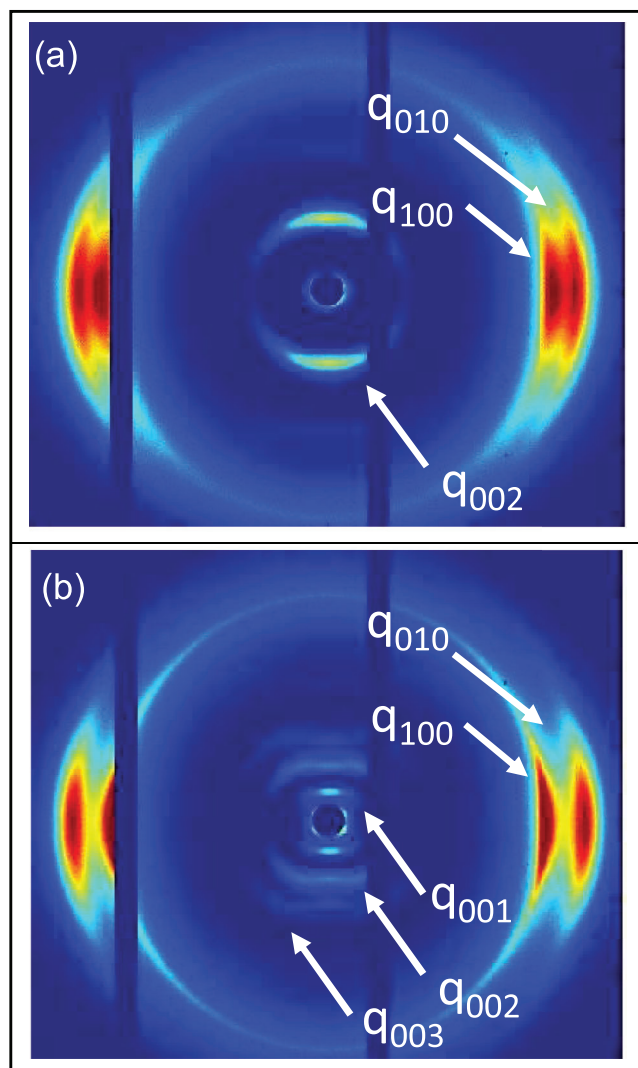


**Figure 7.** Representative 2D XRD pattern of drawn fibers made from a) PA10.12 and b) PA10.18. The most intense reflections are labeled.

## 4. Discussion

### 4.1. Overall Structure of Even-Even PA10. $n$ in the Non-Oriented State

The scattering pattern observed for the investigated PA10. $n$  series after slow cooling near ambient temperature indicate quite similar packing states as observed for many other even-even polyamide samples. The detected  $q_{100}$  and  $q_{010}$  reflections are related to spacings of  $d_{100} = 0.44$  nm and  $q_{010} = 0.37$  nm, respectively. This finding is in accordance with results in the literature<sup>[1]</sup> where similar chain packing is commonly observed for  $\alpha$  and  $\beta$  phases of even-even polyamides.<sup>[7]</sup> In depth studies on differently oriented polyamides and detailed calculations show that these spacings correspond to unit cells with  $a = 0.49$  nm and  $b = 0.54$  nm including an angle  $\gamma$  of about  $63.5^\circ$ . It was demonstrated that these packing states are characterized by hydrogen bonds located within the planes defined by the ac axes. The  $c$  vector is here

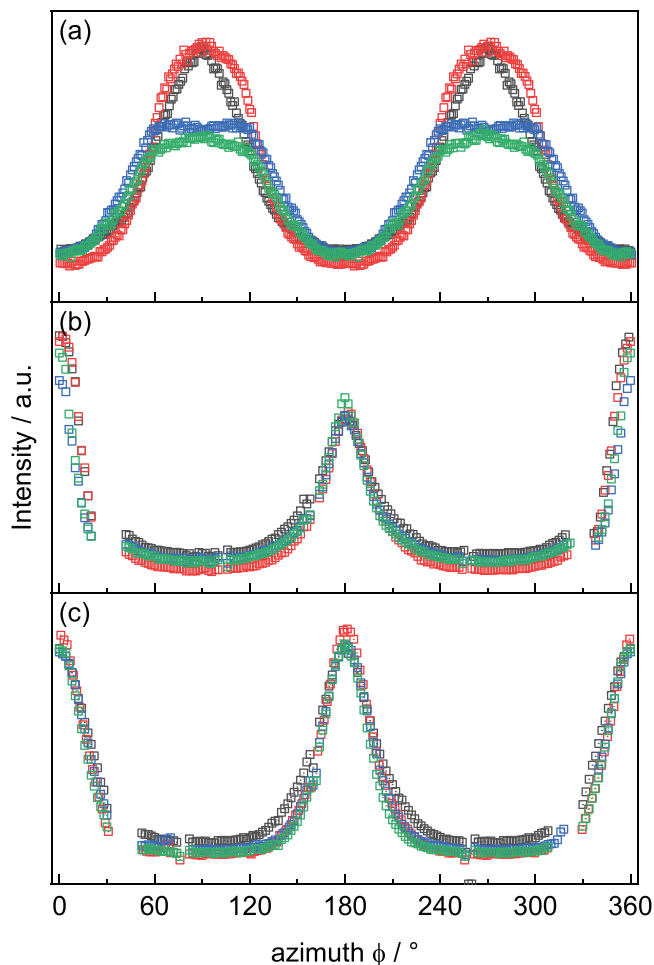


**Figure 8.** Dependence of the scattering intensity on azimuthal angle  $\phi$  for PA10. $n$  (black - 12, red - 14, blue - 16, green - 18). Data for the a) (002), b) (100), and c) (010) reflections are presented.

parallel to the chain axis and its length is often approximated by  $c = (0.125 \cdot N) - 0.02$  nm assuming that the  $\text{CH}_2$  chains are in the all-trans state.  $N$  represents the number of bonds along the entire backbone in a monomer and 0.02 nm is a correction due to the presence of amide groups in the backbone. Differences between different  $\alpha$  and  $\beta$  phases occur basically due to differences in the angle between the layers where the amide “defects” are located relatively to the chain direction  $c$ . In particular, the  $d_{00l}$  spacings for the  $\beta$  phases (monoclinic  $\beta_a$  and triclinic  $\beta_p$ ) should be significantly larger than those for the  $\alpha$  phases (triclinic  $\alpha_p$  or  $\alpha_a$ ) since there is a much more significant tilt between chain axis ( $c$ ) and surface normal of the lattice planes containing the amide groups in the latter. This is reported for various even–even polyamides and is also applicable to the PA10. $n$  series investigated here.

Hence, it is interesting to analyze and compare the spacings  $2 \times d_{002}$  for different series of even–even polyamides in the non-oriented state. A common slope of about  $0.092 \pm 0.003$  nm/ $\text{CH}_2$  unit is observed like for various series in a plot  $2 \times d_{002}$  versus number of methylene units per monomer (Figure 11). This can be interpreted as an indication for the occurrence of a quite similar crystalline phase or—in other words—a similar tilting of the

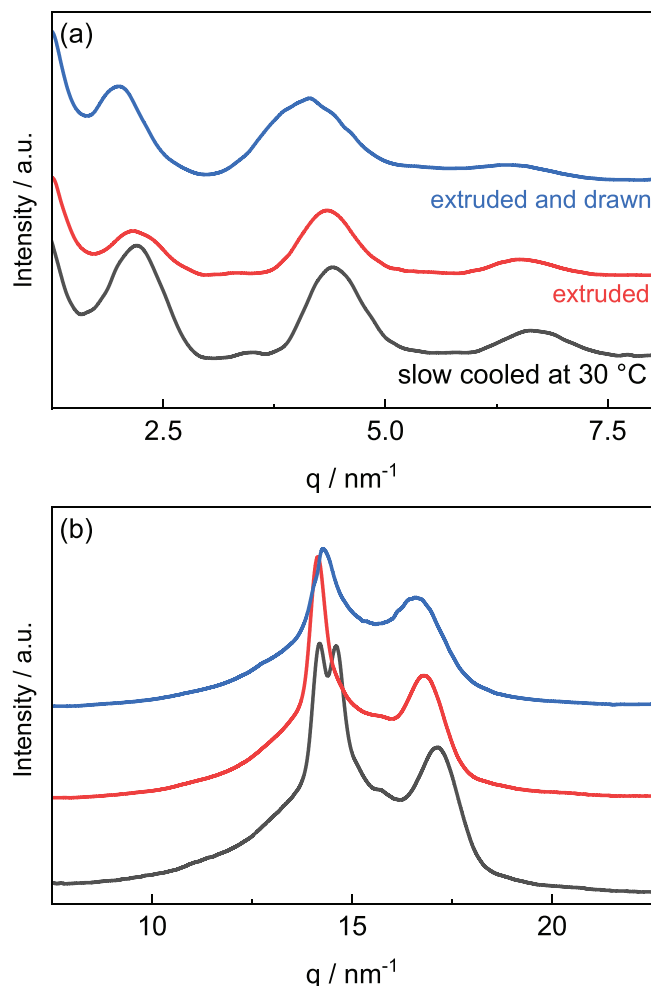


**Figure 9.** X-ray diffraction pattern of PA10.18 measured at 30 °C after slow cooling from melt, on extruded fibers and drawn fibers in the a) MAXS and b) WAXS region.

thin layers containing amide “defects” relative to the chain axis  $c$ . The examples integrated in Figure 11 for comparison are samples occurring in the  $\alpha_p$  (or  $\beta_p$ ) phase under ambient conditions according to the literature.<sup>[7]</sup> The commonly reported angle  $\alpha$  between the vector in the non-hydrogen bonded direction  $b$  to the chain axis  $c$  of about 49° for the  $\alpha$  phase polyamide can already explain the observed slope of  $0.092 \pm 0.003$  nm/ $\text{CH}_2$  unit, which is significantly smaller compared to the slope expected for fully stretched methylene sequences oriented in (001) direction being 0.125 nm/ $\text{CH}_2$  unit. The slope ratio indicates an effective angle of about 47.5° evidencing that  $\alpha$  states dominate in slowly cooled samples. This result is in agreement with reports in the literature.<sup>[1]</sup> However, one should note that even small scatter in the data for the  $d_{00l}$  spacings would result in a significant change in the relevant tilting angle. An additional change of the tilt angle  $\beta$  between  $a$  and  $c$  axis from about 77° to 90° as predicted for differently tilted H-bonds in  $a$  and  $p$  sheets will not change the  $2 \times d_{002}$  spacing much. Hence,  $a$  and  $p$  states are not easy to discriminate and smaller modifications regarding the packing state are usually hard to identify.<sup>[16]</sup> Note that significant differences in the



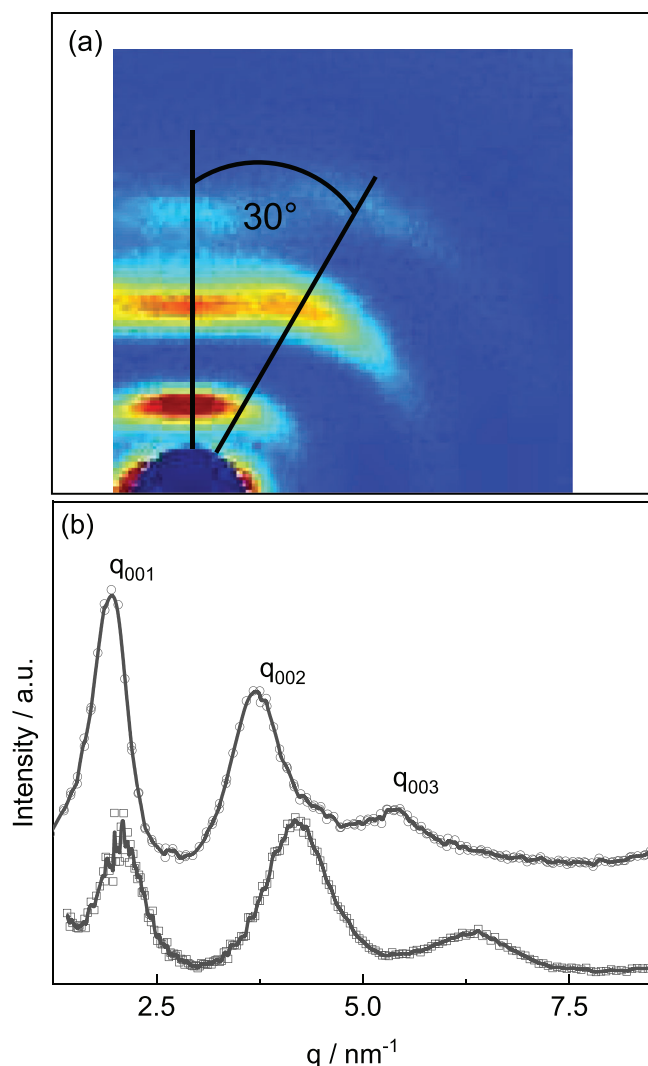


**Figure 10.** a) 2D intensity of PA10.18 in a zoomed view showing the intermediate region. The (00l)<sub>v</sub> and (00l)<sub>t</sub> reflections are indicated by lines. The tilt of the (00l)<sub>t</sub> line relative to the vertical direction is  $\approx 30^\circ$ . b) Intensity of the (00l)<sub>v</sub> and (00l)<sub>t</sub> reflections as function of scattering vector  $q$ . The (00l)<sub>v</sub> reflections are integrated for azimuthal angles between  $85^\circ$  and  $95^\circ$  (○) and the (00l)<sub>t</sub> reflections for angles between  $115^\circ$  to  $125^\circ$  (□).

slope within our series are not really seen although evidences for the coexistence of two polymorphs in the PA10.16 and PA10.18 are observed in the WAXS range in form of an additional splitting of the (100) reflection.

#### 4.2. Structure Formation During Cooling

Considering the overall structure formation process in even-even polyamides during cooling the following scenario seems to be reasonable: The pre-peaks in the MAXS range near  $5 \text{ nm}^{-1}$  commonly observed for molten samples above  $T_M$  clearly indicate that the structure formation starts from an already nanophase-separated melt where methylene sequences and amide groups are basically demixed due to specific interactions. During cooling in lower PA10. $n$  members the  $\gamma$  polymorph is forming at  $T_C$

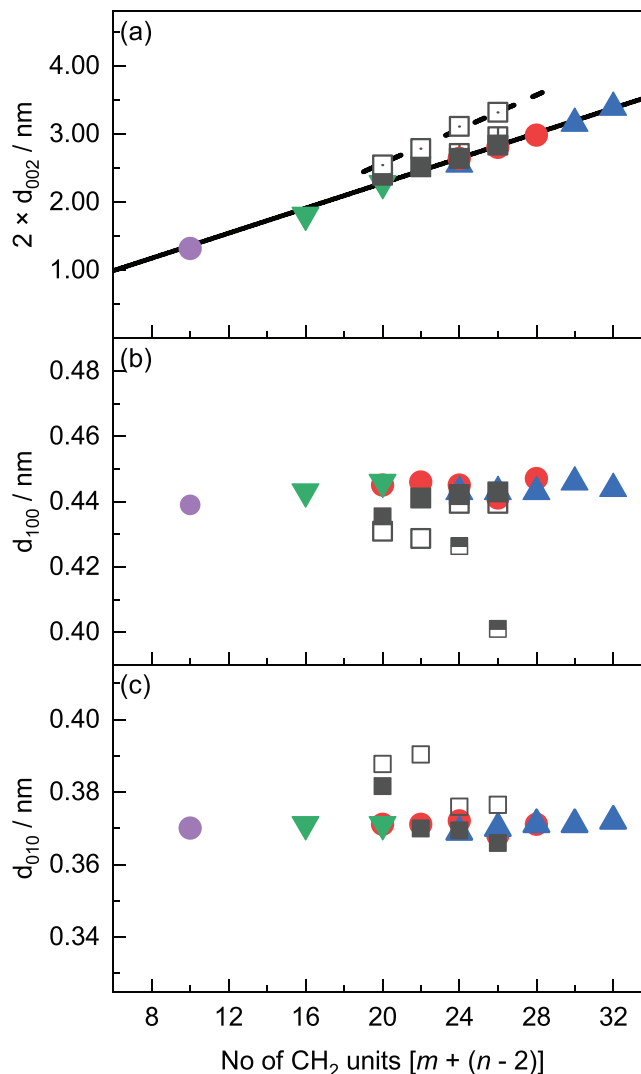


**Figure 11.** Spacings for different series of even-even polyamides as function of the total number of CH<sub>2</sub> units per monomer. The reported values of  $2 \times d_{002}$ ,  $d_{100}$  and  $d_{010}$  for PA10. $n$  from this work (black) are compared with data for PA 6.6 (violet), PA 6.12 and PA 10.12 (green,<sup>[39]</sup>), PA 8.18 to PA 12.18 (red,<sup>[34]</sup>) and PA 4.22, PA 10.22 and PA 12.22 (blue,<sup>[37]</sup>). The  $d_{100}$  spacing of PA10.16 and PA10.18 is represented by half filled squares. The dashed line is an approximation of the  $2 \times d_{002, v}$  values considering the theoretical slope of  $0.125 \text{ nm/CH}_2$  unit for non-tilted fully extended methylene sequences plus an offset of  $0.071 \text{ nm} \pm 0.021 \text{ nm}$  due to the amide groups. The solid line is a linear fit to the  $2 \times d_{002}$  values of the non-oriented polyamides  $m.n$  (slope  $0.092 \pm 0.003 \text{ nm/CH}_2$  unit, intercept  $0.446 \pm 0.0771 \text{ nm}$ ). The full squares represent non-oriented samples, which are measured after cooling from the melt. The open squares are for extruded and drawn PA10. $n$  fibers showing oriented crystals (dot at center for  $\beta$  phase, cross at center for  $\alpha$  phase).

first mainly driven by specific interactions induced by the amide groups forming hydrogen bonds. Already in this state the chain to chain distances are fixed with an area per stem (in planes with a normal parallel to the  $c$  axis) of about  $0.153 \text{ nm}^2$  which is already smaller compared to that in orthorhombic polyethylene crystals ( $0.185 \text{ nm}^2$ ). During further cooling the crystalline state is perfected step by step below the Brill transition temperature

$T_B$ , resulting in an increasing asymmetry of the stem packing in cross-sections perpendicular to the chain axes  $c$  for the low temperature phases  $\alpha$  and  $\beta$ . The average area per stem is not significantly changing. However, it is discussed that the hydrogen bonding situation is significantly changing from out of plane for the  $\gamma$  phase to being located within ac plane for  $\alpha$  and  $\beta$  phases causing more asymmetric packing of the stems. Note that a gradual separation of the  $d_{100}$  and  $d_{010}$  spacings is even observed in samples like PA10.16 and PA10.18 where the  $\gamma$  phase is not observed. This indicates that the asymmetry of stem packing in the thermodynamically stable state systematically increases below  $T_M$ . Below 60 °C this transformation is basically completed for all investigated PA10. $n$  samples and common polymorphs are stable. Numerical simulations suggest that the  $\alpha_p$  phase is the energetically preferred state what is in line the commonly observed situation in experimental studies. However, there is also clear evidence that the energetic differences are quite small between various  $\alpha$  and  $\beta$  polymorphs indicated for example by the often reported coexistence of  $\alpha_p$  and  $\beta_p$  phases.

### 4.3. Influence of Fiber Processing

The X-ray diffraction data of ram-extruded and subsequently drawn fibers show clearly that the crystalline state of the investigated PA10. $n$  series is affected by the processing conditions. This is somehow expected since relevant polymorphs are structurally and energetically quite similar. Considering the  $d_{002, v}$  spacings of PA10.12 and PA10.14, a significant shift to larger values is observed in comparison with  $d_{002}$  of non-oriented samples. This effect is accompanied by a slight distortion in chain packing indicated by the WAXS peak positions. Hence, it is unlikely that this is exactly the same polymorph like that one formed during slow cooling. The (00l) reflections are found in the vertical direction in the 2D pattern indicating lattice planes oriented nearly normal to the main chain direction being parallel to the fiber axis. Similar (00l) peaks in vertical direction are also found (together with another tilted set of reflections) in PA10.16 and PA10.18. Analyzing the dependence of the spacings  $2 \times d_{002, v}$  on  $n$  for all PA10. $n$  fibers (Figure 11) one can observe a slope of about 0.125 nm/CH<sub>2</sub> unit corresponding to methylene sequences in the fully extended all trans state. Hence, it is most likely that this is a  $\beta$  phase, which is basically absent or rarely observed in non-oriented samples. Note that the average difference between  $2 \times d_{002, v}$  and the length of fully stretched length of methylene sequence  $0.125 \text{ nm} \times (m + (n - 2))$  is only  $0.071 \text{ nm} \pm 0.021 \text{ nm}$  being basically the estimated thickness of thin layers containing amide units in chain direction  $c$  for this polymorph. However, a significant scatter is expected in this case due to a limited number of data points.

The  $d_{00l, t}$  spacings related to the reflections tilted in the 2D pattern by about 30° relative to the vertical direction for PA10.16 and PA10.18 fibers are much more similar to those seen for slowly cooled, non-oriented PA10.16 and PA10.18 samples. The WAXS reflections do also occur at very similar positions for oriented and non-oriented samples. Accordingly, it is reasonable to assume that non-oriented PA10. $n$  samples appear preferentially in a triclinic  $\alpha$  phase like reported for many other even–even polyamides.<sup>[1,7]</sup> Note that there are nevertheless indications for

two coexisting phases in slowly cooled non-oriented PA10.16 and PA10.18 samples since there is a clear splitting of the (100) reflections. A certain shoulder is also seen for the (100) reflection of related fiber-oriented samples. Whether or not the two polymorphs occurring in non-oriented as well as oriented PA10.16 and PA10.18 samples are truly identical or only similar remains open at this point. What is evident, however, is that already moderate external forces can change the packing state of PA10. $n$  samples significantly. Even long annealing times do not guarantee that equilibrium phases like observed during slow cooling without application of external forces are seen under ambient conditions after extrusion and/or fiber drawing.

In general, one should keep in mind that the structural differences between different  $\alpha$  and  $\beta$  polymorphs in even–even polyamides are probably very small and mainly related to changes of the tilt of the thin layers with amide “defects” relative to the backbone direction. This means that even weak external forces or small pressure differences can have an influence on the crystal structure formed. A detailed knowledge about the equilibrium phase diagram of even–even polyamides does not exist. That the lengths of the methylene sequences has an influence on the Brill transition from the low temperature  $\alpha$  (or  $\beta$ ) phase to the high temperature  $\gamma$  phase has been reported earlier.<sup>[7]</sup> A shift of the Brill transition temperature  $T_B$  to higher temperatures with increasing length of the methylene sequences is commonly observed. For too long methylene sequences a Brill transition is not detected and  $T_B$  is fictively occurring above the melting temperature of  $\alpha$  or  $\beta$  phase. Exceptional packing states have been only reported in PA 2. $n$  samples.<sup>[7,16]</sup> This may indicate that the  $\gamma$  phase is more dominated by the native packing of the amide groups as compared to the  $\alpha$  and  $\beta$  phases where driving forces related to the methylene sequences are more relevant. Distinct transition temperatures between different low temperature  $\alpha$  and  $\beta$  phases are not (or very seldomly) reported for even–even polyamides. This can be understood as an additional indication for weak energetic differences between these phases but might be also related to complications to differentiate these polymorphic states in non-oriented samples. In any case one has to expect that various factors like pressure, shear forces or water content can influence the polymorphic state favored in even–even polyamides.

Further progress in understanding the occurrence of different polymorphic states in polyamides like those investigated here requires a better knowledge of the relevant thermodynamics. Ideally a phase diagram of the corresponding materials should be available. Although single approaches in this direction have been reported for commercial PA6 and PA11 samples,<sup>[10]</sup> the existing information is extremely limited. Despite of easily accessible transitions like Brill transition at  $T_B$  and melting at  $T_m$ , there is practically no knowledge about thermodynamically important aspects like melting temperatures of  $\alpha$  and  $\beta$  polymorphs, the relation between these phases (enantiotropic or monotropic) and the reasons for the sometimes reported coexistence of the these polymorphs. This applies to the explorative PA10. $n$  samples studied here but also to broadly investigated polyamides like PA66, PA6, or PA12. This calls for experimental studies with methods where structural changes on the way from the melt to a certain crystallization temperature below  $T_m$  and vice versa can be prevented like ultrafast scanning calorimetry. This may allow to

answer the question whether kinetic effects are most important for the coexistence of  $\alpha$  and  $\beta$  fractions or changes in the thermodynamic equilibrium states depending crystal size are relevant like discussed in other cases.<sup>[40]</sup> However, the situation is further complicated by the fact that  $\alpha$  and  $\beta$  states can hardly be discriminated in case of non-oriented samples. Hence, even approaches where rapidly quenched samples can be studied by diffraction methods may have limitations. In order to reach to a better basic understanding of structure formation processes in polyamides in the future these challenges have to be overcome.

In addition to the scientific interest in the phase behavior of even–even polyamides, there are also serious reasons from an applied point of view to control their crystalline state. This is important for various polyamide applications since properties like melting temperature, mechanical strength and ductility can be significantly influenced.<sup>[13–15]</sup> These properties are most relevant for the use of polyamides in high performance components or as fibers. In this respect the existence of systematic trends depending on the molecular architecture might be an alternative strategy for a rational design of polyamide components and semi-finished products with desired properties.

## 5. Conclusions

Structural features of a series of a PA10.*n* series with *n* = 12, 14, 16, and 18 are investigated. It is observed that these samples show very similar polymorphic states like other even–even polyamides. At low temperatures seemingly triclinic  $\alpha$  phase is preferentially formed after slow cooling from the melt for all investigated samples. At high temperatures above the Brill transition at 90 °C a  $\gamma$  phase is found for PA10.12. For PA10.14 a Brill transition is indicated very close to the melting point at 150 °C. All other samples show no  $\gamma$  phase below the melting temperature of the low temperature phases but still significant changes in the stem-to-stem distances approaching  $T_M$  are observed. These findings are consistent with results for other even–even polyamide series in the literature.

Results for fibers containing well oriented crystals show that the polymorphic state observed is truly affected by processing conditions and applied external forces. A  $\beta$  polymorph is observed for all fiber-oriented PA10.*n* samples which is seemingly absent (or a very small fraction) in slowly cooled samples. In addition triclinic  $\alpha$ -like patterns are detected for PA10.16 and PA10.18 corresponding to the states observed in non-oriented samples after slow cooling. Hence, it is concluded that  $\alpha$  polymorphs are preferred in more equilibrated samples under ambient conditions. Moreover, it is discussed that structural and energetic differences between different  $\alpha$  and  $\beta$  polymorphs in even–even polyamides are quite small resulting in an significant influence of external forces on the crystalline state and sometimes coexisting polymorphs. An application relevant consequence is that processing conditions can significantly influence structure and properties of polyamide-based components and semi-finished products. In this respect it is important to note that the molecular architecture of PA10.*n* and even–even polyamides in general can be used to influence and tune their crystalline state due to systematic dependencies on the methylene sequence length.

## Supporting Information

Supporting Information is available from the Wiley Online Library or from the author.

## Acknowledgements

The authors thank Dr. Franz-Erich Baumann for synthesis of the polyamides, Dr. Nasir Mahmood and Dr. Ralf Schlegel for the support in preparing oriented samples, Dr. Heiko Huth for support with DSC measurements as well as Prof. Dr. Thomas Thurn-Albrecht and his work group for collaboration in XRD measurements. Financial support by the DFG within the framework of Sonderforschungsbereich SFB-TRR 102 “Polyamers under multiple constraints” (project B14) is highly acknowledged.

Open access funding enabled and organized by Projekt DEAL.

## Conflict of Interest

The authors declare no conflict of interest.

## Data Availability Statement

The data that support the findings of this study are available from the corresponding author upon reasonable request.

## Keywords

polyamides, polymer crystallization, X-ray diffractions

Received: November 30, 2022

Revised: January 24, 2023

Published online: February 12, 2023

- [1] C. Bunn, E. V. Garner, *Proc. R. Soc. Lond.* **1947**, 189, 39.
- [2] D. R. Holmes, C. W. Bunn, D. J. Smith, *J. Polym. Sci.* **1955**, 17, 159.
- [3] N. A. Jones, E. D. T. Atkins, M. J. Hill, S. J. Cooper, L. Franco, *Macromolecules* **1997**, 30, 3569.
- [4] N. A. Jones, E. D. T. Atkins, M. J. Hill, S. J. Cooper, L. Franco, *Macromolecules* **1996**, 29, 6011.
- [5] M. Kohan, *Nylon Plastics Handbook*, Hanser/Gardener Publications, Cincinnati, OH **1995**.
- [6] L. Bottenbach, R. Binsack, *Kunststoff Handbuch, Band 3/4 Technische Thermoplaste*, Carl Hanser Verlag, Munich **1998**.
- [7] N. A. Jones, E. D. T. Atkins, M. J. Hill, *Macromolecules* **2000**, 33, 2642.
- [8] B. Lotz, *Adv. Fiber Mater.* **2021**, 3, 203.
- [9] Y. Wang, P. Zhu, C. Qian, Y. Zhao, L. Wang, D. Wang, X. Dong, *Macromolecules* **2021**, 54, 6835.
- [10] J. Pepin, V. Miri, J.-M. Lefebvre, *Macromolecules* **2016**, 49, 564.
- [11] C. Ramesh, *Macromolecules* **1999**, 32, 5704.
- [12] J. Pepin, V. Gaucher, C. Rochas, J.-M. Lefebvre, *Polymer* **2019**, 175, 87.
- [13] M. An, Q. Zhang, Y. Lin, D. Wang, W. Chen, L. Meng, P. Yin, L. Li, *Macromolecules* **2020**, 53, 11153.
- [14] K. Jariyavidyanont, S. Mallardo, P. Cerruti, M. L. Di Lorenzo, R. Boldt, A. M. Rhoades, R. Androsch, *Rheol. Acta* **2021**, 60, 231.
- [15] A. M. Rhoades, A. M. Gohn, J. Seo, R. Androsch, R. H. Colby, *Macromolecules* **2018**, 51, 2785.
- [16] B. Lotz, *Macromolecules* **2021**, 54, 551.
- [17] G. Rojas, B. Inci, Y. Wei, K. B. Wagener, *J. Am. Chem. Soc.* **2009**, 131, 17376.

- [18] E. B. Trigg, T. W. Gaines, M. Maréchal, D. E. Moed, P. Rannou, K. B. Wagener, M. J. Stevens, K. I. Winey, *Nat. Mater.* **2018**, *131*, 725.
- [19] X. Zhang, L. Santonja-Blasco, K. B. Wagener, E. Boz, M. Tasaki, K. Tashiro, R. G. Alamo, *J. Phys. Chem. B* **2017**, *121*, 10166.
- [20] P. Ortmann, T. A. Lemke, S. Mecking, *Macromolecules* **2015**, *48*, 1463.
- [21] V. Danke, G. Gupta, S. Reimann, W. Binder, M. Beiner, *Eur. Polym. J.* **2018**, *103*, 116.
- [22] V. Danke, S. Reimann, W. H. Binder, G. Gupta, M. Beiner, *Sci. Rep.* **2020**, *10*, 12119.
- [23] V. Danke, M. Beiner, K. Saalwächter, M. Schäfer, *Macromolecules* **2019**, *52*, 6943.
- [24] M. Ballauff, *Makromol. Chem., Rapid Commun.* **1986**, *7*, 407.
- [25] A. Adam, H. W. Spiess, *Makromol. Chem., Rapid Commun.* **1990**, *11*, 249.
- [26] E. Hempel, H. Budde, S. Höring, M. Beiner, *J. Non-Cryst. Solids* **2006**, *352*, 5013.
- [27] S. Pankaj, M. Beiner, *J. Phys. Chem. B* **2010**, *114*, 15459.
- [28] M. Beiner, K. Schröter, E. Hempel, S. Reissig, E. Donth, *Macromolecules* **1999**, *32*, 6278.
- [29] M. Beiner, H. Huth, *Nat. Mater.* **2003**, *2*, 595.
- [30] P. J. Flory, *Principles of Polymer Chemistry*, Cornell University Press, Ithaca, NY **1953**.
- [31] B. Herzog, M. I. Kohan, S. A. Mestemacher, R. U. Pagilagan, K. Redmond, R. Sarbandi, in *Ullmann's Encyclopedia of Industrial Chemistry*, Wiley, New York **2020**, pp. 1–47.
- [32] G. Gupta, V. Danke, T. Babur, M. Beiner, *AIMS Mater. Sci.* **2017**, *4*, 970.
- [33] H. Arimoto, M. Ishibashi, M. Hirai, Y. Chatani, *J. Polym. Sci. Part A: Gen. Pap.* **1965**, *3*, 317.
- [34] W. Li, D. Yan, *Cryst. Growth Des.* **2006**, *6*, 2182.
- [35] Y. Li, D. Yan, X. Zhu, *Macromol. Rapid Commun.* **2000**, *21*, 1282.
- [36] Y. Li, D. Yan, X. Zhu, *Eur. Polym. J.* **2001**, *37*, 1849.
- [37] G. Zhang, D. Yan, *Cryst. Growth Des.* **2004**, *4*, 383.
- [38] Y. Li, D. Yan, G. Zhang, *J. Polym. Sci., Part B: Polym. Phys.* **2003**, *41*, 1422.
- [39] L. Wang, X. Dong, M. Huang, A. J. Müller, D. Wang, *ACS Appl. Mater. Interfaces* **2017**, *9*, 19238.
- [40] G. T. Rengarajan, D. Enke, M. Steinhart, M. Beiner, *Phys. Chem. Chem. Phys.* **2011**, *13*, 21367.